In Vivo He-3 MR Images of Guinea Pig Lungs[1]

Robert D. Black, PhD
Hunter L. Middleton, PhD
Gordon D. Cates, PhD
Gary P. Cofer, MS
Bastiaan Driehuys, PhD
William Happer, PhD
Laurence W. Hedlund, PhD
G. Allan Johnson, PhD
Mark D. Shattuck, PhD
John C. Swartz, PhD

The authors imaged the lungs of live guinea pigs with hyperpolarized (HP) helium-3 as a magnetic resonance (MR) signal source. HP He-3 gas produced through spin exchange with rubidium metal vapor was delivered through an MR-compatible, small-animal ventilator. Two- and three-dimensional lung images acquired with ventilation-gated, radial k-space sampling showed complete ventilation of both lungs. All images were of high quality, demonstrating that HP He-3 allows high-signal-intensity MR imaging in living systems.

Index terms: Lung, MR, 60.12143 • Magnetic resonance (MR), contrast enhancement, 60.12143 • Magnetic resonance (MR), inert gas imaging, 60.12147

Radiology 1996; 199:867–870

THE ability to optically polarize the nuclei of the inert gases helium-3 and xenon-129 to 30%–50% levels has made available a powerful new signal source for magnetic resonance (MR) imaging examinations. The nonequilibrium nuclear polarization of this hyperpolarized (HP) gas can be as much as 10^4–10^5 times larger than the equilibrium polarization of the hydrogen protons in water used in conventional MR imaging experiments. Even though the spin density of the gases (at 1 atm) is roughly 3,000 times smaller than that of water, this still represents a substantial net gain in signal amplitude. For example, an MR signal obtained in a 2-T field of a volume of He-3 polarized to 30% can yield a signal-to-noise ratio that is an order of magnitude larger than that for an equivalent volume of water.

It is important to note that the signal-to-noise ratio gains for HP gas relative to water assume identical flip angles. The gain in signal per excitation of polarized inert gas relative to that of protons in water is

$$\frac{2k_B T P \omega_g \gamma_g n_g}{\hbar \omega_P^2 \gamma_P n_P}, \qquad (1)$$

where the subscript g denotes gas, p denotes proton, γ is the gyromagnetic ratio for the nuclei, P is the polarization, n is the nucleus number density, ω is the Larmor frequency, T is the spin temperature, k_B is the Boltzmann constant, and $\hbar$ is the Planck constant over 2π.

MR imaging with HP noble gases has shown great promise in recent experiments. In lungs of dead rodents, at MR imaging with He-3 (1) and Xe-129 (2), however, the quantity of gas available was too limited to successfully incorporate the complication of respirating a living animal. These experiments employed small-volume gas cells (~25 mL) with breakable glass seals. The noble gas contained therein was HP through collisional spin exchange with alkali-metal vapor that was optically pumped by a laser. We expanded this technique to be used in gas cells with larger volume (200–600 mL HP gas at standard temperature and pressure) by using high-power diode laser array technology and by redesigning the polarization chambers to allow more controlled release of the HP gas. Both of these advances were necessary to deliver a sufficient quantity of HP gas to allow MR imaging in a living animal.

Not surprisingly, the amount of gas that can be polarized is ultimately limited by the laser power that is available. A useful relation (3) for making estimates is

$$V_{STP} = T_1 R \eta / (n_0 P), \qquad (2)$$

where V_{STP} is the volume of gas at standard temperature and pressure being polarized, n_0 is the density of an ideal gas at standard temperature and pressure (2.7×10^{19} atoms per cubic centimeter), P is the equilibrium polarization of the He-3, T1 is the longitudinal relaxation time that characterizes the rate of decay of the nuclear polarization toward equilibrium, R is the number of laser photons absorbed per unit time, and η is the efficiency with which absorbed photons induce nuclear spin flips. This relation arises from the necessity for an equilibrium between the number of relaxations per unit time ($[n_0 \cdot V_{STP} \cdot P]/T1$) and the number of laser-induced spin flips per time ($R \cdot \eta$). For Xe-129, η is approximately 5% (3), with the majority of the angular momentum lost to rubidium-xenon rotational motion during collisions. On the other hand, He-3 is polarized at a higher temperature (ie, greater rubidium density) of approximately 180°C, where there is an additional loss of angular momentum to rubidium-rubidium collisions, which reduces η to a few tenths of a percent (4). For a given temperature, η will still be constant, however, so the volume of gas that can be polarized is proportional to R, which is generally proportional to the laser-output power. Diode laser arrays can provide an increase in laser power that is more than an order of magnitude above that provided by the argon ion and titanium-sapphire laser combination used in earlier experiments (1). The incorporation of such arrays into the optical pumping process is very important for production of HP He-3 gas in volumes of a few hundred cubic centimeters (5,6).

As a result of the increased volume of gas necessary to respirate a living animal, a more controlled delivery method was needed than was provided by the simple breakable glass seal formerly used to allow HP gas out of the glass polarizing chamber. We achieved this method by replacing the breakable glass seals with a glass valve. Although this was a seemingly innocuous change, the presence of a gasket and other materials necessary for the operation of a valve could have interfered with the polarization process, by reducing the average T1 of the volume of HP gas within the pumping chamber (7). With the available laser power, a T1 of approximately 10 hours is necessary to allow buildup of high polarizations in the He-3 gas (8). With use of the valved polarization chamber, we could administer a controlled dosage of HP gas without expending the whole volume in a single bolus. Furthermore, we found that these polarization chambers could be

[1] From the Center for in Vivo Microscopy (R.D.B., G.P.C., L.W.H., G.A.J., M.D.S.) and the Department of Physics (J.C.S.), Duke University Medical Center, Durham, NC; and the Department of Physics, Princeton University, Princeton, NJ (H.L.M., G.D.C., B.D., W.H.). Received December 11, 1995; revision requested January 26, 1996; revision received February 12; accepted February 27. Supported by National Institutes of Health grant P41-RR05959, National Science Foundation grant CDR-8622201, Air Force Office of Scientific Research grant F49620-92-J-0211, Advanced Research Projects Agency grant DAMD17-94-J-4469, Army Research Office grant DAAH04-94-0204, and the Schering-Plough Research Institute. **Address reprint requests to** Elaine G. Fitzsimons, Education Coordinator, Center for in Vivo Microscopy, Rm 141 Bryan Research Bldg, Box 3302 DUMC, Durham, NC 27710.

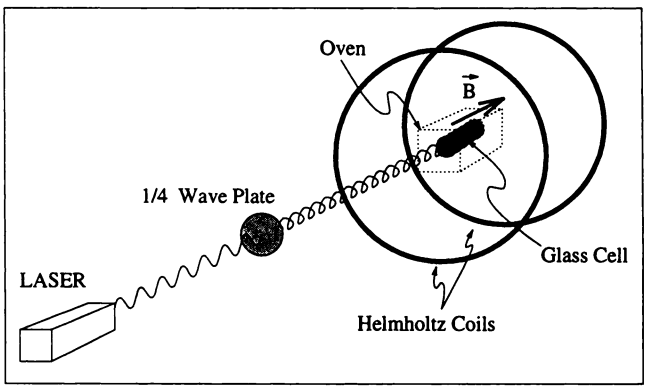

Figure 1. Schematic depicts the optical pumping apparatus. The Helmholtz coils provide the 7.5-G field used during pumping. The one-quarter (*1/4*) wave plate converts the linearly polarized light from the diode laser to circularly polarized light (*B*).

refilled without substantial deterioration in the T1 associated with the chamber, which suggests that use of a continuous-flow polarization chamber may be viable in the future.

Materials and Methods

The HP gas production system centered around the long-T1 polarizing chambers. These chambers contained 8 bar He-3, about 100 mbar nitrogen, and 10–20 mg rubidium metal. The internal volumes of the pumping chambers varied from 20 to 75 cm^3, so the net volumes of gas at standard temperature and pressure varied between 200 and 600 cm^3. One chamber at a time was placed in a 7.5-G magnetic field (Fig 1) and heated to about 180°C to create a sufficiently dense rubidium vapor ($\sim 3 \times 10^{14}$ atoms per cubic centimeter). The beam from a diode laser array tuned to the 795-nm D1 transition in rubidium was passed through a quarter-wave retardation plate, and the resulting circularly polarized beam was used to illuminate the pumping chamber along the axis of the magnetic field. The angular momentum in the circularly polarized laser beam was transferred to the alkali valence electron where subsequent gas-phase collisions with the He-3 transferred some of this polarization to the He-3 nuclei (9,10). The output power of the diode laser was about 8 W (continuous wave) when tuned to the rubidium resonance. The one important draw back of these lasers is their extremely broad spectral output, roughly 1,000-GHz full width at half maximum. But with the 8 atm of helium present in the chamber, the alkali-metal absorption line was sufficiently broadened to allow absorption of a substantial fraction of the laser light. After they were polarized for 15–20 hours, the HP samples were carried a few hundred meters (in the earth's magnetic field only) to the gas delivery system.

The HP gas production system was fitted with a pulsed MR system used to measure the relative polarization in the pumping chamber. This system operated at 24 kHz with a flip angle sufficiently small, approximately 5°, to induce no meaningful polarization loss during a pulse. Because this was only a relative measurement, the exact He-3 polarization was not known but was estimated to be approximately 10%.

All images were acquired on a 2-T, 30-cm-diameter-bore, horizontal magnet with shielded coils capable of producing gradients to 18 G/cm. The radio-frequency (RF) coil was an 8-cm-diameter birdcage design (11), tuned to the He-3 frequency (~65 MHz). Anatomic landmarks were used to align the animal within the coil and the magnet before the gas was introduced. The gradient and RF system were controlled by using a console (Signa 5.4; GE Medical Systems, Milwaukee, Wis) interfaced to the RF system by means of an intermediate frequency mixer.

Male 350–500-g guinea pigs (Hartley; Charles River Laboratories, Wilmington, Mass) were anesthetized with intraperitoneally administered butorphanol (3 mg per kilogram of body weight) and methohexital sodium (Brevital Sodium [45 mg/kg]; Lilly, Indianapolis, Ind) along with atropine sulfate ([0.35 mg/kg]; Vedco, St Joseph, Mo). The animal study protocol adhered to the institutional review board guidelines of Duke University. A gas-tight airway was established by performing a tracheostomy with a 14-gauge catheter (Intracath; Becton Dickinson, Rutherford, NJ). The animals were then ventilated with an MR imaging–compatible ventilator modified with two valves (Fig 2), which allowed automatic switching between two gas mixtures: (*a*) the regular breathing mixture of isoflurane (Aerrane [1%–2%]; Ohmeda Caribe, Guayama, Puerto Rico) and air, or (*b*) HP He-3. The He-3 gas was delivered via a glass syringe in all examinations. Time-series data indicated that the container maintained the polarization of the gas for the duration of imaging. The breathing rate was 35–45 breaths per minute, the tidal volume was 3–6 cm^3, and the heart rate was 215–220 beats per minute. Electrocardiographic electrodes were taped to the foot pads and a thermistor probe (Yellow Springs Instruments, Yellow Springs, Ohio) was inserted into the rectum. The electrocardiogram, body temperature, and airway pressure were monitored continuously (12). Scans were gated on the ventilation cycle (data acquisition started after the completion of the He-3 inspiration); no cardiac gating was used. The imaging parameters were designed so that all the available gas was used up.

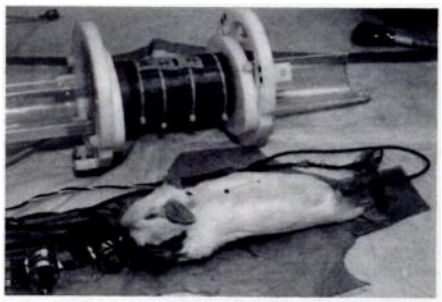

Figure 2. Photograph depicts the breathing and switching valves used to alternately deliver He-3 or air with isoflurane to the subject animal, which is under general anesthesia.

Results

Two- and three-dimensional images were acquired, with use of a ventilation-gated radial acquisition sequence (13). Views, or specific vectors in the time-domain space (k space), were acquired for each image. In two-dimensional imaging, the initial section-selective excitation produced a free induction decay that was rephased by means of a second gradient along the section-selective axis. The strong gradients available on the system permitted this refocusing in less than 600 msec. The resulting free induction decay was encoded by means of projection gradients along the remaining two axes. The effective delay between the end of the RF excitation and the first data point sampled was thus minimized and this, in turn, limited the potential loss of signal and resolution arising from diffusion (14,15).

All of the RF pulses used in the acquisitions were of equal magnitude. The amount of magnetization remaining after n pulses of angle θ is roughly, $\cos(\theta)^n$. We made no attempt to collect multiple free induction decays from the same excitation, as dephasing occurs very rapidly. And, of course, no meaningful signal was garnered from the equilibrium magnetization of the He-3 gas. The available signal became smaller after each successive pulse, so the radial views acquired varied in signal intensity. The views were acquired in ran-

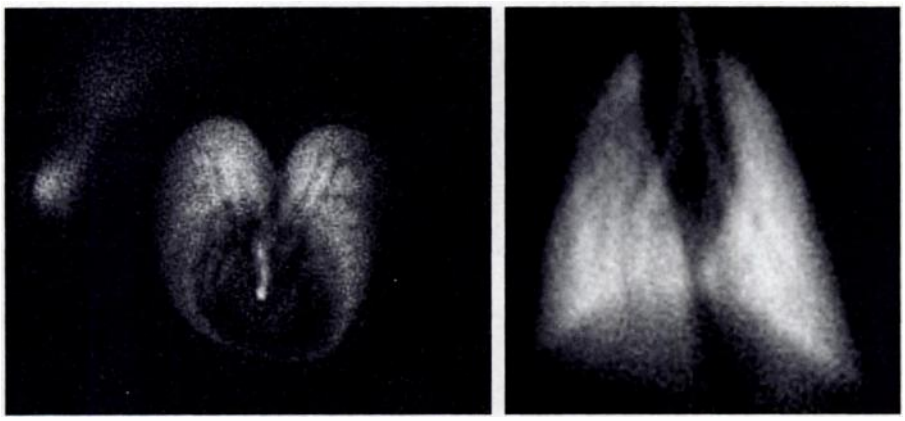

a. b.

Figure 3. Two-dimensional He-3 MR images were obtained in **(a)** axial and **(b)** coronal orientations, with 400 × 400-μm in-plane resolution.

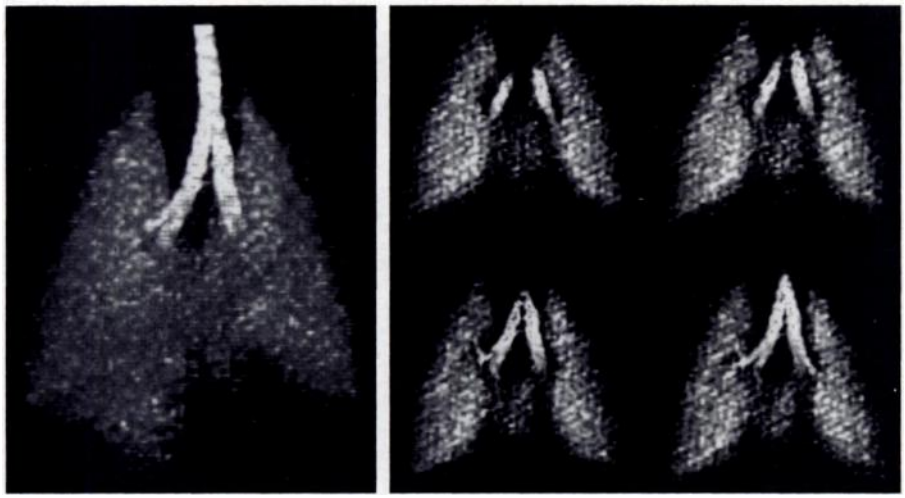

a. b.

Figure 4. He-3 MR images depict **(a)** volume-rendered image from a three-dimensional data set and **(b)** individual sections from the same data set.

dom order, and this helped to smooth out the intensity artifact. The self-diffusion coefficient of He-3 is roughly 2 cm^2/sec. Of course there is no structure within the airways, so the effective resolution is determined by the ability to image gas within a bounded passageway.

Figure 3a and 3b show, respectively, axial and coronal images (no section selection) obtained in separate MR imaging examinations in different animals. In Figure 3a, a 10° RF flip angle was used for 2,048 views (128 radial views per ventilation cycle). He-3 ventilation was alternated with air and anesthetic gas, with images acquired only during He-3 ventilation. The in-plane image resolution was 400 × 400 mm, and no section selection was used. Note the absence of signal intensity in the area where the heart is located. The lung air spaces appear to be completely filled with He-3. The endotracheal tube and trachea can be seen superimposed on the hypointense cardiac area. The plume of signal outside the animal (leftmost edge of Fig 3a) is HP He-3 that escaped from the exhalation port of the breathing valve.

Figure 3b was acquired with an 8° RF flip angle for 1,024 views (128 views per He-3 breath). As in Figure 3a, it is clear that the signal is restricted to the lung, trachea, and major bronchi. The repetition time (time between RF excitations) was 10 msec in both Figure 3a and 3b, and the delay time between the end of the RF excitation and the start of data acquisition was 600 μsec.

Figure 4a is a volume-rendered image from a three-dimensional data set that was acquired with an 8° RF flip angle for 400 views per breath, over 32 breaths of He-3. Figure 4b shows individual sections from that same three-dimensional data set. The voxel size is 400 mm (isotropic). The repetition time was 3.6 msec, and the delay time to the start of data acquisition was 200 msec. The highest signal intensity is seen in the trachea and bronchi. Airway branching can be traced to the third generation. Cartilaginous ring structures are evident in the extrapulmonary airways.

Discussion

The quality of these preliminary images clearly demonstrates that HP He-3 enables high-signal MR imaging in living systems. HP inert gas in MR imaging acts as a wholly different type of "contrast agent," in that it is the signal source (unlike gadolinium compounds, for instance, that act to alter T1). Furthermore, the He-3 is in a nonequilibrium state, so there is no polarization recovery time needed between individual RF excitations. Thus, fast-acquisition techniques are readily applicable. On the other hand, there is only a finite amount of magnetization to work with in a given charge of polarized gas. Also, the rapid diffusion of the spins in the gas phase limits image resolution and may make conventional spin-echo formation difficult.

Because HP gas is not polarized by the magnet used for imaging, the signal-to-noise ratio of the image—assuming the image noise is dominated by Johnson noise from conductive biologic fluids in the sample and not by the MR receiver—is independent of the imaging field strength. To see this, the nuclear MR signal level from HP gas is

$$\frac{n\gamma\hbar P\omega}{2}, \qquad (3)$$

whereas that for the equilibrium signal in a conventional MR imaging experiment is

$$\frac{n\gamma\omega^2\hbar^2}{4k_BT}, \qquad (4)$$

where n is spin number density, γ is the gyromagnetic ratio, $\hbar$ is the Planck constant over 2 π, P is the polarization, ω is the Larmor frequency, k_B is the Boltzmann constant, and T is temperature. The root-mean-square for thermal noise voltage from biologic fluid at a given frequency is proportional to ω (16). Thus it is clear from Equation (3) that the voltage signal-to-noise ratio is independent of ω and from Equation (4) that there is a linear field dependence of image signal-to-noise ratio in conventional MR imaging. This fact means that low-field-strength imaging systems will be very attractive for use in HP-gas MR imaging.

We have started research into the use of HP gas in animal models of airway disease. The independence of the magnetization from restrictions in recovery time will enable dynamic imaging of the inflow and outflow of gas. It is likely that regional measures with helium gas will be more sensitive than traditional global (functional) metrics. The ability to increase the production rate of polarized gas by using high-power, inexpensive diode laser arrays has also enabled us to perform preliminary imaging tests in humans. Results in these preliminary tests will allow assessment of the utility of this technology in the diagnosis of human pulmonary disease. ■

Acknowledgments: The authors gratefully acknowledge the technical assistance of Brian Saam, PhD, Robert Guenther, PhD, and Michael Souza at Princeton University, and the technical assistance of Tracy Dense, BS, Ted Wheeler, BS, VMT, and the editorial assistance of Elaine Fitzsimons, MS, at Duke University.

References

1. Middleton H, Black R, Saam B, et al. MR imaging with hyperpolarized ^{3}He gas. Magn Reson Med 1995; 33:271–275.
2. Albert M, Cates G, Driehuys B, et al. Biological magnetic resonance imaging using laser-polarized ^{129}Xe. Nature 1994; 370:199–201.
3. Bhaskar N, Happer W, McClelland T. Efficiency of spin exchange between rubidium spins and ^{129}Xe nuclei in a gas. Physics Review Letters 1982; 49:25–28.
4. Knize R. Spin destruction in a rubidium-rubidium and potassium-potassium collision. Physics Review A 1989; 40:6219–6222.
5. Wagshull W, Chupp T. Optical pumping of high-density Rb with a broadband dye laser and GaAlAs diode laser arrays: ^{3}He applications to polarization. Physics Review A 1989; 40:4447–4454.
6. Cummings W, Häusser O, Lorenzon W, Swenson D, Larson B. Optical pumping of Rb vapor using high-power $Ga_{1-x}Al_xAs$ diode laser arrays. Physics Review A 1995; 51:4842–4851.
7. Fitzsimmons W, Tankersley L, Walters G. Nature of surface-induced nuclear-spin relaxation of gaseous ^{3}He. Physics Review 1969; 179:156–165.
8. Gamblin R, Carver T. Polarization and relaxation processes in ^{3}He gas. Physics Review A 1965; 138:946–960.
9. Bouchiat M, Carver T, Varnum C. Nuclear polarization in ^{3}He gas induced by optical pumping and dipolar exchange. Physics Review Letters 1960; 5:373–375.
10. Chupp T, Wagshul M, Coulter K, McDonald A, Happer W. Polarized high-density gaseous ^{3}He targets. Physics Review C 1987; 36:2244–2251.
11. Hayes CE, Edelstein WA, Schenck JF, Mueller OM, Eash M. An efficient, highly homogeneous radiofrequency coil for whole body NMR imaging at 1.5 T. J Magn Reson 1985; 63:622–628.
12. Hedlund LW, Johnson GA, Mills GI. Magnetic resonance microscopy of the rat thorax and abdomen. Invest Radiol 1986; 21:843–846.
13. Gewalt SL, Glover GH, MacFall JR, Hedlund LW, Johnson GA. MR microscopy of the rat lung using projection reconstruction. Magn Reson Med 1993; 29:99–106.
14. Callaghan PT, Eccles CD. Diffusion-limited resolution in nuclear magnetic resonance microscopy. J Magn Reson 1988; 78:1–8.
15. Ahn CB, Cho ZH. A generalized formulation of diffusion effects in μm resolution nuclear magnetic resonance imaging. Med Phys 1989; 16:22–28.
16. Black RD, Early TA, Roemer PB, et al. A high temperature superconducting receiver for NMR microscopy. Science 1993; 259:793–795.

Application of Region-of-Interest Imaging Techniques to Neurointerventional Radiology[1]

Stephen Rudin, PhD
Lee R. Guterman, PhD, MD
William E. Granger, BS
Daniel R. Bednarek, PhD
Leo N. Hopkins, MD

To reduce radiation exposure to patients and staff during neurointerventional procedures, region-of-interest (ROI) techniques were used with fluoroscopy, road mapping, and digital subtraction angiography in 19 patients. ROI filters, made of multiple layers of gadolinium, were attached to the collimators. Patient skin exposure was reduced by a factor of 3.3–10.0 across 85% of the field of view, and exposures were reduced to below thresholds for skin effects.

Index terms: Diagnostic radiology, radiation exposure • Radiations, exposure to patients and personnel

Radiology 1996; 199:870–873

[1] From the Department of Radiology, Division of Radiation Physics (S.R., D.R.B.), and the Departments of Neurosurgery (S.R., L.R.G., D.R.B., L.N.H.) and Biophysical Sciences (S.R., W.E.G., D.R.B.), the School of Medicine and Biomedical Sciences, University at Buffalo, State University of New York, Erie County Medical Center, 462 Grider St, Buffalo, NY 14215, and the Millard Fillmore Hospitals, Buffalo, NY. From the 1995 RSNA scientific assembly. Received December 15, 1995; revision requested January 18, 1996; revision received February 9; accepted February 12. Supported in part by National Institutes of Health (National Institute of Neurological Disease and Stroke) grant R01NS31883. **Address reprint requests to** S.R.

REGION-OF-INTEREST (ROI) radiographic imaging techniques (1) involve the placement of a beam-attenuating filter with an aperture between the x-ray source and the patient. The aperture is located to project a higher intensity x-ray beam over the features of interest while features peripheral to this ROI are viewed with reduced intensity and reduced image quality. This results in a substantial reduction in patient dose, which can decrease the risk of both stochastic and deterministic effects. Stochastic effects are a particular concern in general diagnostic procedures since a large number of such procedures are performed. Deterministic effects are a greater concern in interventional procedures because their length can cause the dose to exceed the threshold of 2 Gy (200 rad) for erythema and epilation or other serious skin effects (2,3). ROI techniques can reduce the skin dose over a large fraction of the field of view (FOV), as well as reduce the effective dose equivalent (4).

Beam-shaping techniques (1,5–9) change the size, shape, or intensity distribution of the x-ray beam by means of collimation or ROI filters. Use of these techniques may be justified in interventional radiology to reduce the entrance exposure to most of the FOV because often only a small region near the interventional site must be imaged with maximal image quality. Outside of this ROI, the image is used mostly for reference, rather than in the direct guidance of the intervention. In this peripheral area, the presence of increased quantum noise due to reduced photon fluence may be acceptable.

Other methods that may be used to reduce exposure during interventional procedures include uniform beam filtration; removal of the grid; automatic brightness control curves, which emphasize higher peak kilovoltages; use of larger optical irises; and implementation of low-pulsed-rate fluoroscopy or temporal averaging. All these methods, however, involve some degradation of the entire image FOV. For example, uniform copper filtration across the entire field, altering the automatic brightness control curve toward higher peak kilovoltages or the acceptance of more scatter would substantially reduce radiographic contrast of vessels. Use of low-pulsed-rate fluoroscopy or temporal averaging will reduce the temporal resolution. There may be times during interventional procedures when full-field degradation may be acceptable (10,11), but their use would have to be weighed against the possible increased risk of untoward events. Dose reduction of an order of magnitude can be achieved with use of combinations of these techniques (11). ROI techniques are compatible with all of these full-field methods and may be used simultaneously when appropriate.

In this preliminary clinical study, we provide the results of application of the ROI method to three modes of operation in human neurointerventional procedures: unprocessed ROI fluoroscopy,